Catal Lett (2010) 134:228–232
DOI 10.1007/s10562-009-0250-2

Adsorption Dynamics of CO on Silica Supported Gold Clusters: Cluster Size Effects in Molecular Beam Scattering Experiments

E. Kadossov · U. Burghaus

Received: 27 October 2009 / Accepted: 24 November 2009 / Published online: 5 January 2010

Abstract We report on particle size effects in the adsorption dynamics (gas-surface energy transfer) of CO, studied by molecular beam scattering. The initial adsorption probability shows a maximum as a function of Au exposure, χ_{Au}, i.e., cluster size. This reactivity maximum appears to coincide with the enhancement of catalytic activity seen for the CO oxidation reaction for small clusters.

Keywords Molecular beam scattering · Dynamics · Kinetics · CO · Nanogold · Nanoclusters

1 Introduction

Although the nanogold system has been studied extensively in catalysis and surface science, [1–4] few studies have focused on the effect of supported nano-size gold metal clusters on gas-surface energy transfer processes (adsorption dynamics) [5–8]. However, the adsorption of gas-phase species is always the first step in heterogeneously catalyzed surface reactions, and this certainly influences the entire reaction mechanism and product formation rates. Perhaps the simplest way to explore these effects is to measure the initial adsorption probability, S_0, which quantifies the zero coverage reactivity of a catalyst towards the adsorption of a given gas-phase species. S_0 is determined by gas-surface energy transfer processes. In this letter, we utilized supersonic molecular beam scattering techniques to measure S_0 for silica supported Au clusters.

One of the most important prototype surface reactions is the conversion of CO to CO_2. The time dependent CO concentration, [CO], on the catalyst surface is given by

$$d[CO]/dt = S_0F - k_d[CO]k_r[CO][O], \quad (1)$$

where k_d, k_r, [O], and F are the desorption rate coefficient, the reaction rate coefficient, the oxygen concentration, and the CO flux, respectively. Irrespective of the simplicity of this particular scheme, which does not directly include a possible oxygen activation or collaborative effects (e.g., oxygen stabilized CO), it is evident that an effect of the gold clusters on the CO-to-surface energy transfer processes (i.e., on S_0) also affects the CO_2 product formation rates, R_{CO2}. For example, variations in S_0, dependent on the exposure time (i.e., the amount of Au), χ_{Au}, or the morphology of the gold clusters, result in variations in the effective flux, given by S_0F, which drives the oxidation reaction. A large effective flux leads to a large CO concentration on the surface (see Eq. (1)), and hence, to a large CO_2 product formation rate, given by:

$$R_{CO2} = k_r[CO][O].$$

Thus, besides the interest in revealing mechanistic details, the gas-surface energy transfer processes, quantified by determining S_0, distinctly affect R_{CO2}, which is important for applications. This conclusion does not qualitatively change with the use of a more complicated kinetics mechanism.

Indeed, the experiments reported here revealed a distinct effect of the gold cluster morphology on S_0. The average size of the supported gold clusters has been determined by statistical analysis of scanning electron microscopy (SEM) images. $S_0(\chi_{Au})$, with χ_{Au} for the Au exposure, showed a

E. Kadossov · U. Burghaus (✉)
Department of Chemistry, Biochemistry, and Molecular Biology, North Dakota State University, Fargo, USA
e-mail: uwe.burghaus@ndsu.edu
URL: www.chem.ndsu.nodak.edu

maximum for gold clusters of about 3.5 nm, which appears to agree with the cluster size dependent enhancement seen for R_{CO2} in prior studies [1, 2, 4, 9, 10]. The growth of the vapor deposited gold clusters (supported on silica) and their interaction with CO has been characterized further by Auger electron spectroscopy (AES) and thermal desorption spectroscopy (TDS). Some related data have been presented previously, see ref. [11].

2 Experimental Procedures

The measurements were conducted using a home-built, triply-differentially pumped molecular beam scattering apparatus [12]. The supersonic beam was attached to a scattering chamber, which contained a mass spectrometer, an AES system, a sputter gun, and an electron beam metal evaporator. Gold was vapor deposited on silica at a surface temperature of 300 K. The impact energy, E_i, of the CO molecules could be varied within (0.09–0.91) eV by seeding 3% CO in He, combined with a variation of the nozzle temperature between 300 and 750 K. The heating rate for the TDS experiments was 2 K/s. The reading of the thermocouple was calibrated in situ by TDS measurements of condensed alkanes. The silica support was cleaned by Ar^+ sputtering and annealing in O_2 at 1,100–1,200 K, following previously published procedures [13]. Scanning electron microscopy (SEM) images were collected at Argonne National Laboratory with a JEOL JSM-7500F and at Brookhaven National Laboratory with a Hitachi S-4800 UHR. The resolution of the SEM images was about 1–2 nm. For the statistical analysis, commercial imaging analysis software (Pixcavator IA 4.2) was used. The cluster numbers given refer to a frame size of 7.3×10^4 nm^2. The particle densities were obtained by averaging over 310×235 nm.

3 Data Presentation and Discussion

A characterization of the Au growth mode and adsorption kinetics of CO is given in Figs. 1, 2, 3. Figures 4, 5 summarize the molecular beam scattering data, which provide new insights into the CO-to-Au/SiO_2 energy transfer processes governing the efficiency of the adsorption dynamics of CO on the nanogold system.

The gold AES peak intensity and the Au-to-oxygen AES line intensity ratio is given as a function of Au exposure time, χ_{Au}, in Fig. 1. (The oxygen signal originates from the silica support.) As is often observed (e.g., see ref. [14] for Au/SiO_2 or ref. [12, 15] for Cu/ZnO), the slopes of these curves change with χ_{Au}, indicating a variation in the growth mode of the Au cluster. In agreement with prior

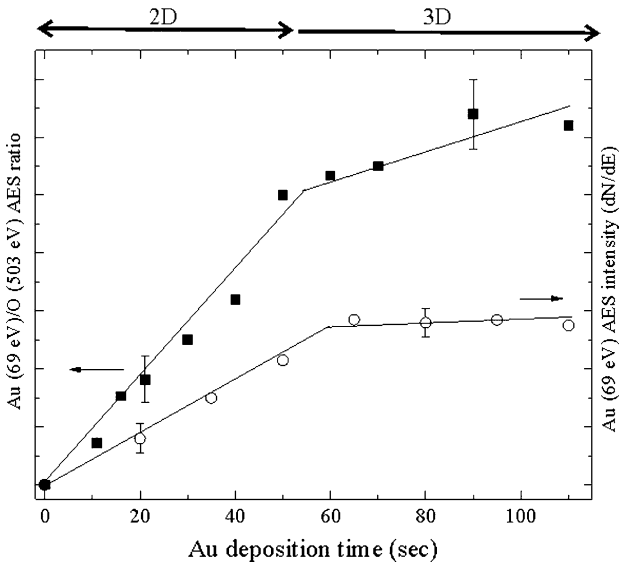

Fig. 1 AES intensity as a function of Au deposition time: (*solid squares*) Au (69 eV)/O (503 eV) ratio; (*open circles*) Au (69 eV) intensity. (The error bars are derived from the noise level of the AES spectra, taking into account that an intensity ratio is depicted)

studies, [13, 14] one can conclude that Au initially formed small two-dimensional (2D) clusters, which grew into wider and taller three-dimensional (3D) structures with increasing Au exposure. Therefore, due to screening effects, the AES intensity increased more slowly with χ_{Au} after 3D clusters began to form.

The conclusions drawn from the AES data are supported by the statistical analysis of SEM images. Figure 2a depicts SEM images of the silica support after depositing $\chi_{Au} = 10$ s Au at room temperature. The cluster size distribution was narrow and centered at 3.5 nm (see Fig. 2b). (The sizes of the nearly circular clusters given in Fig. 2 are equivalent diameters of a circle which has the same area as the imaged clusters.) According to STM (scanning tunneling microscopy) studies, [16] increasing χ_{Au} initially results in an increase in the cluster density while keeping the cluster size fairly constant (nucleation regime). Thus, Fig. 2a should be representative of the Au cluster morphology for small exposures (up to 10 s, see discussion below). Annealing this sample for 10 s at 950 K led to the cluster morphology depicted in Fig. 2c. The small Au clusters sintered, forming larger clusters with sizes of up to 40 nm. The Au cluster density dropped roughly by a factor of two, from 5.3×10^{11}/cm^2 (Fig. 2a) to 2.4×10^{11}/cm^2 (Fig. 2c), while annealing the sample.

Before discussing the effect of the Au growth morphology on the adsorption dynamics, on which this study is focused, a brief discussion of the TDS data characterizing the adsorption kinetics is useful. Figure 3 shows a set of TDS curves obtained when the surface was saturated with CO at 100 K. The amount of deposited Au has been

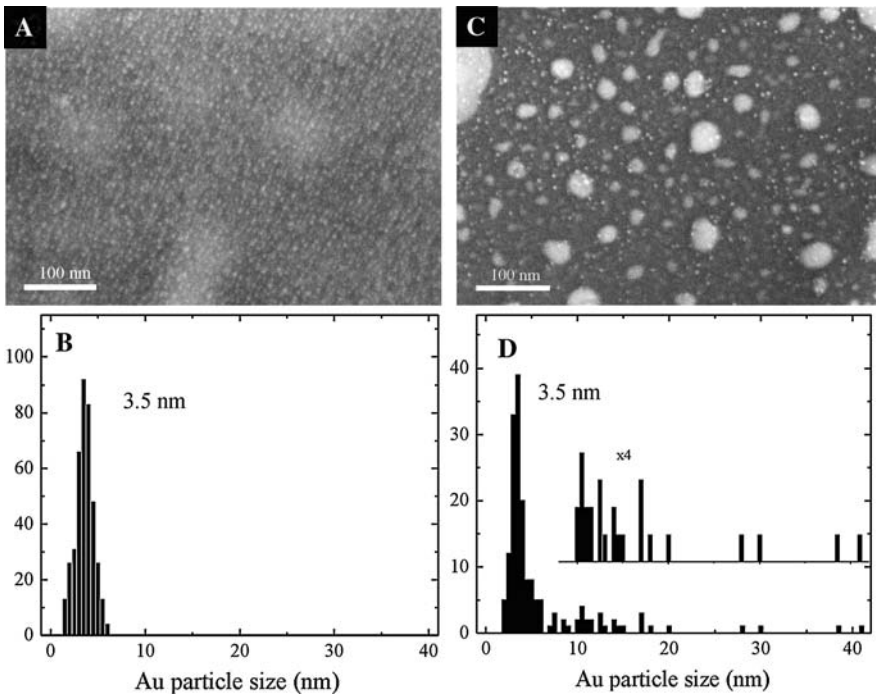

Fig. 2 SEM images of Au/SiO_2 with Au deposition time 10 s: **a** before annealing; **c** after annealing to 950 K; **b** and **d** statistical analysis. (The contrast of the image (**a**) has been enhanced.)

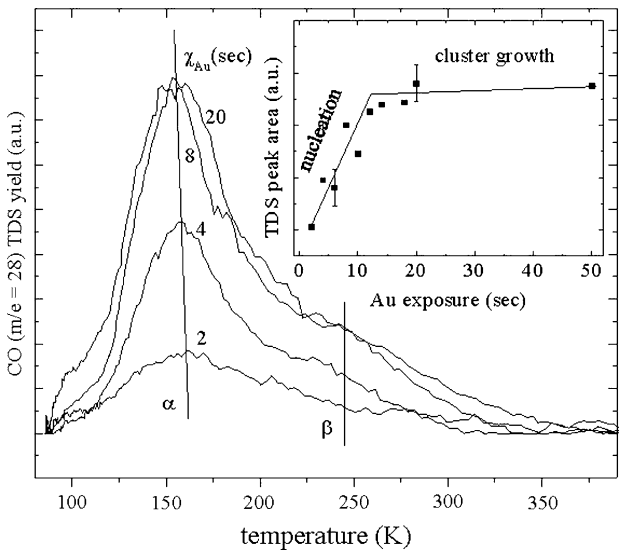

Fig. 3 TDS spectra of 4 L CO adsorbed on Au/silica, as a function of Au deposition time. The inset shows the corresponding TDS peak areas. (The error bars are calculated from the integrated count rates—TDS areas—using common statistical formula.)

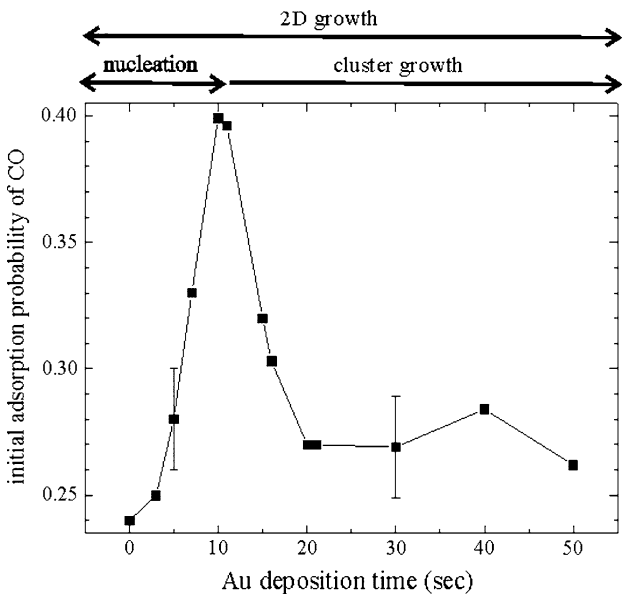

Fig. 4 Initial adsorption probability of CO as a function of Au deposition time at 93 K. Kinetic energy of CO, E_i, amounted to 0.39 eV. (Three independent experimental runs have been averaged using two different silica supports. The uncertainties have been calculated from the noise level of the transients and by averaging the independent experimental runs.)

increased up to a maximum of $\chi_{Au} = 50$ s. Thus, according to the AES data (Fig. 1) and STM studies, [14] the equivalent Au coverage was below 1 ML and Au was present as 2D clusters. Two CO TDS peaks appeared at about 150 K (α peak) and 250 K (β peak). The inset of Fig. 3 shows the integrated CO TDS intensity as a function of χ_{Au}, demonstrating the dependence of the total amount of adsorbed CO on χ_{Au}. In agreement with the TDS data shown here, in most studies on Au model catalysts utilizing TDS, [10, 17–19] IR (infrared spectroscopy), [20] XPS (X-ray photoelectron spectroscopy), [19] and STM, [19, 20] universal kinetics of CO adsorption have been seen, which are fairly independent of the support [10, 17]. Typically, two features are present in TDS and one IR peak has been detected. These results, in most cases, have been related to

CO adsorption on low-coordinated sites of the Au clusters [10, 17, 21]. Prior DFT (density functional theory) calculations indicated CO adsorption on sevenfold and sixfold coordinated sites as the energetically most favorable adsorption sites, which may be associated with on-top adsorption of CO on Au step edges and kink sites of Au clusters [17]. Adsorption on terrace sites, flat adsorbed CO, and CO bonded to bridge sites along steps have been ruled out. The DFT calculations also reproduced the presence of only one IR structure [17]. Accordingly, smaller Au clusters are more reactive than larger clusters, which led to leveling out of the total amount of adsorbed CO already at $\chi_{Au} = 10$ s (see inset of Fig. 3). The total number of adsorption sites is proportional to the cluster's surface area and certainly increases with increasing cluster density and size. Therefore, initially (within the Au cluster nucleation regime), the CO TDS intensity increased upon deposition of more gold on the support. At larger Au exposures, the CO TDS intensity leveled out. In this gold exposure range, the decrease in the fraction of low-coordinated sites started to dominate over the increase in the total number of adsorption sites [22]. Please note that this exposure range is beyond the nucleation regime, but below the formation of extended 3D clusters. The AES, SEM, and TDS data provided a robust characterization of the Au/SiO_2 sample studied and were consistent with what is known from the literature.

Figure 4 depicts the initial adsorption probability, S_0, as a function of Au deposition time, χ_{Au}. Interestingly, the $S_0(\chi_{Au})$ curve showed a maximum at $\chi_{Au} = 10$ s. Data from three independent experimental runs were averaged, dropping the statistical error in S_0 to ± 0.02. The variation in $S_0(\chi_{Au})$ amounted to $\Delta_{max}S_0(\chi_{Au}) = 0.15 \pm 0.04$ or 40%. The SEM image in Fig. 2a shows a sample for $\chi_{Au} = 10$ s; i.e., this morphology, with 3.5 nm Au clusters, corresponded to the maximum seen in $S_0(\chi_{Au})$. As already described in the introduction, the maximum in S_0 for 3.5 nm Au clusters also would generate a maximum in CO_2 formation rates, which agrees with the well-known cluster size dependent enhancement of the catalytic activity of nanogold [1, 2, 4].

The explanation that we propose is rather straightforward: during the nucleation stage ($\chi_{Au} < 10$ s) of the Au clusters on the silica support, the cluster density increases rapidly with χ_{Au}, as evident from prior STM studies [16]. Therefore, S_0 (see Fig. 4) increases initially with χ_{Au} as the number of catalytically active sites increases (nucleation regime). This effect is conceptually opposite to the well-known site blocking effect [23] caused by catalyst poisoning, where S_0 drops due to the blocking of catalytically active sites. Here we form more catalytically active sites and S_0 initially increases.

However, increasing χ_{Au} after the nucleation regime (and within the 2D cluster growth range) results in an increase in the cluster size, but the cluster density remains essentially constant [13, 16]. Thus, the fraction of low-coordinated gold sites decreases and S_0 decreases [22]. In other words, large 2D Au clusters are less reactive than small ones (see inset of Fig. 3 and refs. [10, 17]). Therefore, S_0 decreases for $\chi_{Au} > 10$ s.

The variation in $S_0(\chi_{Au})$ nicely reflects the variation in the density of catalytically active sites on the clusters.

The stability of the catalyst is interesting from a fundamental perspective, as well as being pertinent for technical applications. Some of the most common mechanisms of catalyst deactivation are sintering effects; i.e., the agglomeration of small clusters to larger clusters at high reaction temperatures over the lifetime of the catalyst. If the model proposed here is correct, annealing of the Au/SiO_2 sample should lead to a decrease in S_0 caused by sintering. Indeed, supporting small Au clusters ($\chi_{Au} = 10$ s) on silica and annealing this sample stepwise up to 950 K leads to a drop in S_0, again by about 40% (see Fig. 5). The SEM image reproduced in Fig. 2c shows an annealed sample. As is evident while the sample is annealed, the cluster size indeed increases from 3.5 nm (Fig. 2b) up to 40 nm (annealed sample, Fig. 2d), and the cluster density decreases. Thus, the molecular beam scattering data shown in Figs. 4, 5 are fully consistent and support the model whereby measurements of S_0 allow for matching of the density of catalytically active sites. Furthermore, the annealing temperature at which S_0 drops ($\sim$600 K, Fig. 5) is close to the Tammann temperature (668 K $\sim$0.5 of the melting temperature) of gold. The

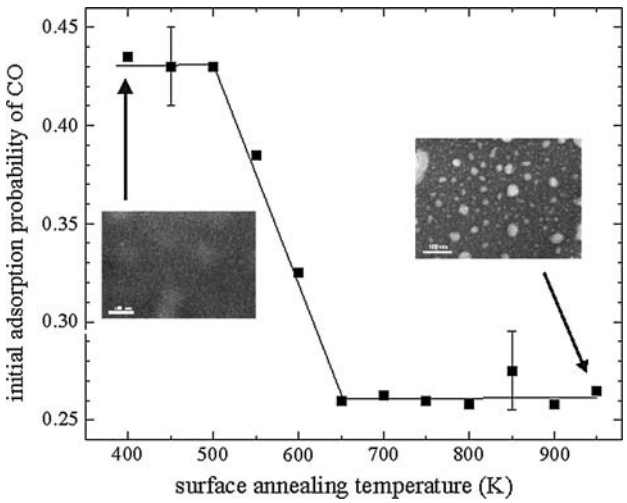

Fig. 5 Initial adsorption probability of CO as a function of Au/SiO_2 annealing temperature. Au deposition time was 10 s, measuring temperature 93 K, $E_i = 0.39$ eV

Tammann temperature is related to the start of the volume diffusion and is sometimes used as an estimate of the sintering threshold temperature [24, 25].

4 Summary

The Au/SiO_2 system has been characterized by AES, SEM, and CO TDS. Interestingly, and as the main result of our study, S_0 versus Au exposure curves show a maximum for Au cluster sizes of 3.5 nm. This effect will also influence product formation rates. In addition, annealing of the supported Au clusters leads to a decrease in S_0, due to sintering effects. Many factors will determine the catalytic properties of the system; however, most studies focus on the kinetics and electronic properties of nanogold. Effects of the adsorption dynamics, although rather small in the case considered here, so far have been mostly overlooked.

Acknowledgments Financial support by an NSF-CAREER award (CHE-0743932) is acknowledged. We thank M. Lu, now at Brookhaven National Laboratories, for the electron microscopy images.

References

1. Haruta M (1997) Catal Today 36:153
2. Choudhary TV, Goodman DW (2002) Top Catal 21:25
3. Zhou B, Hermans S, Somorjai GA (eds) (2004) Nanotechnology in Catalysis, Springer series: nanostructure science and technology, Springer, ISBN 0-306-48323-8
4. Heinz U, Landman U (eds) (2007) Nanocatalysis (NanoScience and Technology) Springer, ISBN 978-3-540-74551-8
5. Kim TS, Stiehl JD, Reeves CT, Meyer RJ, Mullins CB (2003) J Am Chem Soc 125:2018
6. Stiehl JD, Kim TS, McClure SM, Mullins CB (2004) J Am Chem Soc 126:1606
7. Stiehl JD, Kim TS, Reeves CT, Meyer RJ, Mullins CB (2004) J Phys Chem B 108:7917
8. Lee S, Fan C, Wu T, Anderson SL (2004) J Am Chem Soc 126:5682
9. Valden M, Lai X, Goodman DW (1998) Science 281:1647
10. Lemire C, Meyer R, Shaikhutdinov S, Freund HJ (2004) Angew Chem Int Ed 43:118
11. Kadossov E, Justin J, Lu M, Rosenmann D, Ocola LE, Cabrini S, Burghaus U (2009) Chem Phys Lett 483:250
12. Wang J, Burghaus U (2005) J Chem Phys 122:044705
13. Wallace WT, Min BK, Goodman DW (2005) J Mol Catal A 228:3
14. Luo K, Kim DY, Goodman DW (2001) J Mol Catal A 167:191
15. Campbell CT (1997) Surf Sci Rep 27:1
16. Min BK, Wallace WT, Santra AK, Goodman DW (2004) J Phys Chem B 108:16339
17. Yim WL, Nowitzki T, Necke M, Schnars H, Nickut P, Biener J, Biener MM, Zielasek V, Al-Shamery K, Kluener T, Baeumer M (2007) J Phys Chem C 111:445
18. Winkler C, Carew AJ, Haq S, Raval R (2003) Langmuir 19:717
19. Zhao Z, Diemant T, Rosental D, Christmann K, Bansmann J, Rauscher H, Behm RJ (2006) Surf Sci 600:4992
20. Lemire C, Meyer R, Shaikhutdinov S, Freund HJ (2004) Surf Sci 552:27
21. Mavrikakis M, Stoltze P, Norskov JK (2000) Catal Lett 64:101
22. Schimpf S, Lucas M, Mohr C, Rodemerck U, Bruchner A, Radnik J, Hofmeister H, Claus P (2002) Catal Today 72:63
23. Burghaus U, Ding J, Weinberg WH (1997) Surf Sci 384:L869
24. Golunski SE (2007) Platinum Met Rev 51:162
25. University of Oulu, Finland, Retrieved 2009 http://herkules.oulu.fi/isbn9514269543/html/x546.html